Artero-Guerrero, J. A., Varas, D., Pernas-Sánchez, J., & López-Puente, J. (2018). Experimental analysis of an attenuation method for hydrodynamic ram effects. Materials & Design, 155, 451-462.

https://doi.org/10.1016/j.matdes.2018.06.020

Experimental analysis of an attenuation method for Hydrodynamic Ram effects

J.A. Artero-Guerrero[a,*], D. Varas[a], J. Pernas-Sánchez[a], J. López-Puente[a]

[a]*Department of Continuum Mechanics and Structural Analysis. University Carlos III of Madrid. Avda. de la Universidad, 30. 28911 Leganés, Madrid, Spain*

Abstract

The hydrodynamic ram (HRAM) phenomenon occurs when an object with a high-kinetic energy impacts against a fluid-filled structure, which could induce important damages. An attenuation technique would be of great interest for structures which could be subjected to impact. In this work, honeycomb panels are used to fill the entire space inside the structure in such a way that they are able to alleviate the loading onto it. Experimental tests were carried out varying aluminium honeycomb cells orientation, to determine the configuration that mitigates more efficiently the effects of HRAM comparing the results with a non-protected structure. The experimental tests were analysed using a high speed video camera, strain gauges, residual displacement of the structure walls and the deformation of the honeycomb panels. It is shown that for all the configurations, the honeycomb is able to reduce the plastic deformation of the structure. The honeycomb allows to reduce the cavity expansion in the fluid, which is the most dangerous phenomenon in the studied cases. The best configuration is able to diminish up to a 54% the residual expanded volume in the structure walls, and hence considerably

*Corresponding author.
Email address: jartero@ing.uc3m.es (J.A. Artero-Guerrero)

attenuating the HRAM effect on the structure.

Keywords: Hydrodynamic Ram, Attenuation method, Fluid-structure interaction, Fluid-filled tank, High Velocity Impact, Experimental test

1. Introduction

The Hydrodynamic Ram (HRAM) phenomenon occurs when an object with high kinetic energy penetrates a fluid-filled container. The object, while travels through the fluid, transfers part of its energy to it, and consequently to the surrounding structure. Hence the walls of a fluid-filled structure, subjected to an impact load, have to withstand higher energy levels than the same structure without fluid. Therefore it is important to take into account the presence of fluid inside a structure because it is the responsible for increasing the risk of a catastrophic failure [1]. Thus, the HRAM phenomenon is considered one of the most important factors in aircraft vulnerability [2, 3]. Fuel tanks can be impacted by different kind of fragments and in different situations. Different impactors such as hail [6, 7], bird [8] or tyre fragments [9] could impact fuel tanks with enough kinetic energy to generate the HRAM phenomenon causing a catastrophic failure, as happened in the accident of the Concorde [10]. Also, the accidental explosion of an engine can generate a number of fragments that impact at high velocity against the wing fuel tanks [5] producing the HRAM effects as happened in Qantas A-380 accident [4]. The commercial aircraft industry is greatly concerned about this type of Uncontained Engine Rotor Failure (UERF) events. But the HRAM phenomenon is not an unique issue in the aerospace industry, also it is important and should be taken into account in the industrial sector, where a structure containing fluid (vessel, tanker truck, etc.) can be hit at high velocity [11, 12, 13]. This case can

be particularly dangerous if the fluid inside the container is a hazardous material.

The first researches concerning the HRAM were carried out by military agencies in the 70s. It's not until the 90's when academic institutions had studied this phenomenon, applied to commercial aircraft. The HRAM has been analysed experimentally [1, 14, 15], numerically [16, 17, 18, 19] and with analytical models [20]. An extensive review regarding the studies performed can be found in the experimental and numerical works of D. Varas et al. [1, 16]. Additionally to these works, the authors of the present research have published several articles concerning the study of this phenomenon in metallic and composite tubes filled with water [17, 21, 22, 23].

Previous studies have shown that the HRAM phenomenon consists of four main stages: shock, drag, cavity and exit [1, 16, 15, 17]. Each stage contributes to the structural damage through a different mechanism and to a different extent. In addition, depending on the particular circumstances (dimensions of the structure, material and kinetic energy of the object that impacts...), the importance of each stage varies. Shock phase is usually described as one of the main cause of failure for large containers [14] or in the case of low-strength impactors. However when the size of the cavity is similar to the size of the tube, cavity stage becomes the main cause of deformation and failure of the tank.

The conclusions obtained from the previous works are the basis to propose improvements in the vulnerability of fluid-filled tanks subjected to the HRAM phenomenon. It has to be remarked that the works in which HRAM attenuation

methods have been proposed are very scarce. In 1983 A. Copland [24] evaluated the ability of different inerting agents to attenuate HRAM in armoured vehicles. Two different containers were impacted by 12.7 mm AP bullets and 11.9 mm steel spheres. The results indicate that the destructive effects of HRAM may be enhanced by the addition of the inerting agent called "Explosafe" to liquid containing cells, while the addition of the foam studied delayed the pressure pulse and reduced its value contributing to attenuate the effects of HRAM. Other passive fuel tank inerting systems can be found in the work of S. McCormick et al. [25] where a review about both fuel tank fillers and systems which surround the fuel tanks is presented. The work is focused on the capability of different systems to suppress fire in and from ground combat vehicles fuel tanks. D. Townsend et al. [26] used two different techniques in order to reduce the shock pressure waves which are generated in HRAM: thin air-filled baffles introduced inside the fuel tank and bubbling air through the fluid. These two techniques consist in introducing low impedance solutions and hence disrupt or disperse the shock wave produced in the fluid by the projectile impact. The mitigation effect for both techniques reaches approximately a 50 % of reduction in the pressure wave in some region of the fuel tank, and therefore it decreases the damage induced in the structure. Another work that proposed an attenuation technique is the one developed by Peter J. Disimile et al. [27]. In this case, it has been also analysed the mitigation of shock waves using wedged bars placed inside the water filled tank. These elements are specially designed to reduce the shock pressure wave by the destructive interference between the original pressure wave and its reflections. It is shown that the proposed technique allows reducing the pressure measured in the sensors inside the fuel tank up to a 60 %. These two works successfully reduced the shock

pressure wave and therefore the damage induced in the structure. However, as it was said previously, depending on the studied impact conditions and the structure characteristics in which the HRAM is generated, the shock pressure wave may not be the most damaging stage.

The cavity expansion can be considered as the major cause of deformation and failure in the tanks in which the size of the cavity generated inside the tank is similar to the size of the mentioned tank [22, 23]. Theses cases could occur in high velocity impacts of metallic fragments against small range aircrafts or fighters. Therefore, in this work it is proposed an attenuation method focused in the reduction of the cavity expansion, instead of the reduction of pressure waves. In this case, a honeycomb structure is placed inside the fluid filled tank, so that when the cavity grows inside the tank, the honeycomb structure gets deformed plastically, absorbing part of the energy transferred into the fluid. It is well known the high energy absorption to density ratio of honeycomb or lattices structures [28, 29, 30, 31, 32], consequently, it is expected that the structure protected with honeycomb will be subjected to a less damaging loading case. As it is well known honeycomb low density will not counteract with the effort in reducing the weight on aircraft structures. The different orientation possibilities, in which the honeycomb structure can be placed inside the tank, are analysed in order to obtain the best configuration to attenuate the HRAM effects on the structure when it is impacted perpendicularly.

2. Experimental description of the problem

2.1. Experimental set-up

In this work, an experimental set-up has been used to carry out the tests in which the performance of the HRAM attenuation method proposed is analysed. Fig. 1 shows a sketch of the experimental devices used to accomplish and register adequately the tests. All the experimental tests were done at the University Carlos III of Madrid Impact Laboratory.

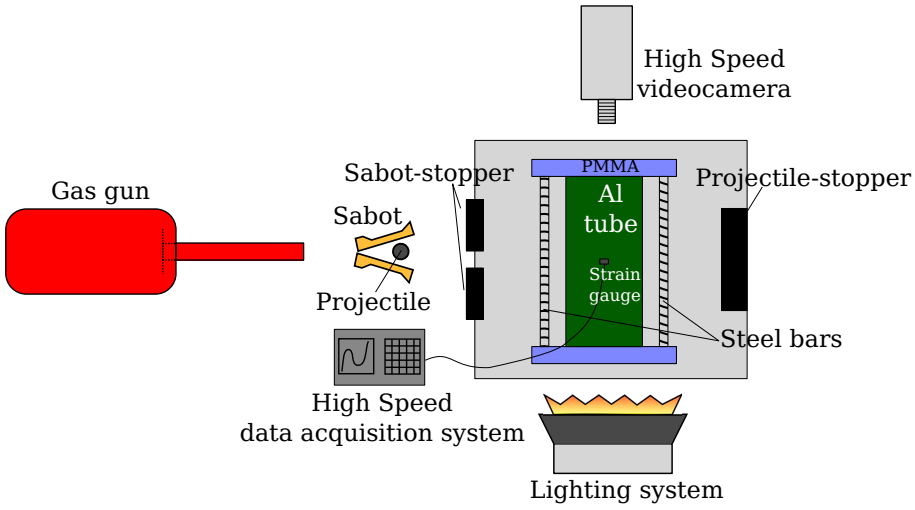

Figure 1: Sketch of the experimental set-up used

The structure analysed is a 6063-T5 aluminium tube (150 *mm* × 150 *mm* × 750 *mm* and 3 *mm* thickness) that has been filled with fluid to study the HRAM effects. According to the recommendations of the Advisory Group for Aerospace Research and Development (AGARD) [2, 3] no fuel was used in any of the experimental tests due to the risk of fire; replacing it with water. The tubes are closed by two PMMA windows (30 *mm* thick) allowing the recording of the impact process.

Four steel bars joint the PMMA and the tube without pre-stressing it; therefore it is needed to use a sealant in the contact between the tube and the PMMA to assure the water tightness of the tube. This set-up is based firstly in the work of Nishida et al. [33], and then modified by D. Varas et al. [1].

The projectile used was a tempered steel sphere (12.5 mm diameter and 8 g of mass and at least $\sim$ 60 HRc). Its geometry helps to the repeatability of the test and due to its high strength no deformation can be seen after the test, so the energy absorbed by the projectile can be neglected. The projectile was launched at 900 m/s by a one-stage light gas gun, manufactured by Thiot Enginierie. The gas gun uses helium that is pressurize up to 270 bar to accelerate the projectile. The barrel is 4.5 m long and its calibre is 25 mm; due to the diameter differences between barrel and projectile the use of a sabot is needed. The sabot is designed to be opened in two valves. A steel structure stops the valves of the sabot preventing its impact against the tube, and allows the impact of the projectile in the tank. After the projectile perforates the whole tube, a thick metal plate is used to stop it, preventing also the possible rebounds.

As it can be seen in Fig. 1 the impact process has been recorded by means of a high speed camera Photron Ultima APX-RS. Based on previous tests performed, a frame rate of 36000 fps was used, which is enough to observe adequately both the projectile entry and perforation of the tube. As it was already said two PMMA windows (closing the tube) were used to allow the recording of the impact process inside the fluid, nevertheless it is worth to mention that two of the honeycombs configurations used to attenuate the HRAM effects impeded viewing the inside of

the tube. However, the video is used to register the impact velocity and the cavity evolution when no honeycomb is added. This kind of tests, in which impacts at high velocity occurs, requires a proper lighting system; moreover taking into account the shutter used of $1\mu s$. In this case an Arrisun 12 Plus lamphead with a 1200 W Hydrargyrum Medium-arc Iodide (HMI) lamp was used.

The aluminium tubes were instrumented with six strain gauges. Two of them were located in the entry wall, near and far from the impact point (G1 and G2 respectively). Another two were placed in the exit wall at the same position as the entry ones (G3 and G4, near and far from the impact point respectively) and the last two gauges were located in the center of the lower and upper wall (G5 and G6) (see Fig. 2). A high speed acquisition system Dewetron DEWE-800 was employed to register all the strain gauges data, using a sample rate of 1 MHz, as well as to synchronise the data with the video recording.

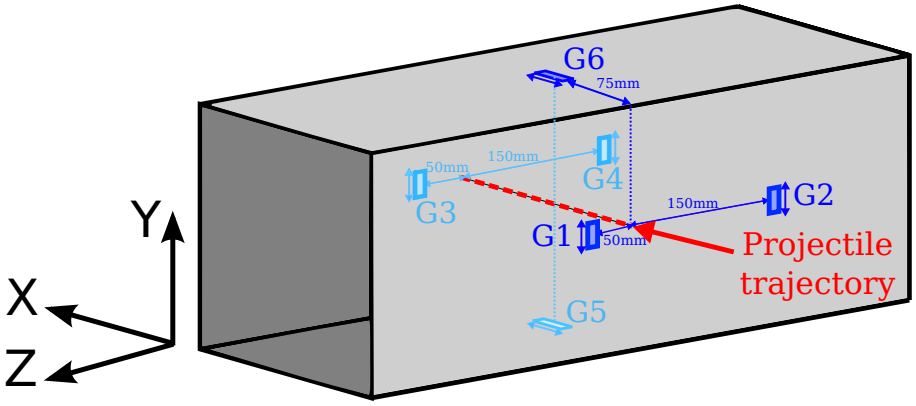

Figure 2: Sketch of the gauges locations

2.2. *Description of the HRAM attenuation method*

As it is said previously, this work proposes a method to attenuate the effects of the HRAM phenomenon and hence reduce the vulnerability of fluid-filled structures. The work is focused on fluid-filled structures in which, due to its dimensions, the most damaging process of the HRAM is the cavity expansion as was observed in previous works [1, 16]. Therefore the method proposed should be able to reduce the cavity formed in order to diminish its load onto the walls structure, and hence the damaging effects. The solution tested and studied consists in placing a honeycomb structure inside the tube. It is expected that the honeycomb panels could reduce the cavity expansion, dissipating through deformation the energy transferred by the fluid and hence alleviating the structure loading.

The honeycomb structures used consist of 5052 aluminium 50 *mm* thickness panels, with a cell size of 6.35 *mm* and a nominal foil thickness of 63.5 μm. The honeycomb geometrical parameters have been selected to maximize its resistance but assuring a low density and a correct filling and circulation of the water inside it. There are three possible configurations of the honeycomb structure depending on how the cells are oriented inside the tube, Fig. 3. In the first configuration, denoted as C-1, the honeycomb cells are placed perpendicularly to the impact direction (X axis) and oriented to the largest dimension of the tube (Z axis). Since the honeycomb panel thickness used is 50 *mm*, 15 panels of 150 $mm \times 150$ *mm* are needed to fill the whole tube. In the second configuration, C-2, the honeycomb cells are oriented in the same direction as the projectile trajectory (X axis), being needed only three panels of 750 $mm \times 150$ *mm*. In the third case, C-3, honeycomb cells are placed perpendicularly to the projectile trajectory (as in the case C-1),

but now they are oriented to the third dimension of the tube (Y axis), therefore three panels of 750 $mm \times 150$ mm are required, as happened in C-2. The three configurations have been tested and analysed in order to decide which one is able to produce the best attenuation effects on the walls structure, comparing it with a non-protected case. To this end, an impact test on a filled tube without the honeycomb structure inside was also performed. Results presented concern to one impact test for each configuration. Variability for cavity evolution, deformation and strain data has been considered negligible attending to the repeatability on previous tests done for aluminium tubes subjected to HRAM events [1].

It has to be mentioned that the weight added by the proposed solution has been taken into account. Due to the very low density of honeycomb (83.2 kg/m^3), the attenuation structure only represents a 6.8% of the aluminium tube-fluid system. In addition the honeycomb could be implemented only in some zones that, due to its position, are statistically more likely to be subjected to different kind of impacts avoiding a catastrophic failure. Therefore the added mass would not be a great disadvantage.

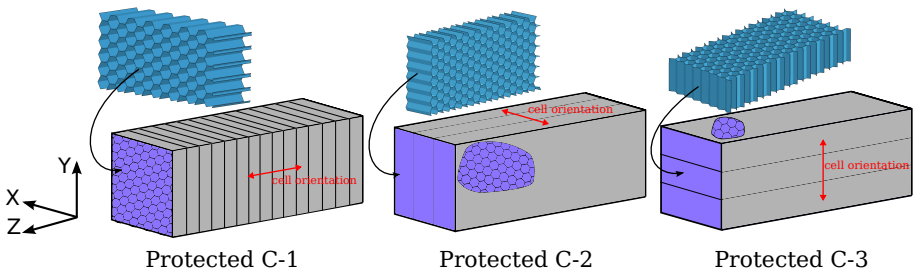

Figure 3: Sketch of the protected configurations

3. Results

In this section the results of the non-protected aluminium tube and the three different protected tubes configurations are presented. Firstly, the images obtained by the high speed camera are studied in order to obtain some qualitative comparison of the HRAM phenomenon between the non-protected and protected tubes. Then the residual deformation and the strain gauge data of the aluminium tube walls are used to compare the HRAM attenuation effect of each configuration.

3.1. High speed video sequence

Some selected frames obtained from the high speed camera for the impact in the non-protected tube and the C-1 protected tube are shown in Fig. 4. As it was already mentioned, the honeycomb cells orientation in the other two configurations (C-2 and C-3) impedes viewing the inside of the tube and therefore the images have not been presented. However, the video sequence images of Fig. 4 can be used to qualitatively compare both cases in the first instants and observe if some remarkable change in the impact process happens in the protected case.

Fig. 4 shows how the cavity is formed in the wake of the projectile once it penetrates the entry wall. This is very clearly observed in the non-protected case, whereas in the case with the honeycomb protection, the cavity can be seen as a kind of non-defined shadow. The projectile impact generates a pressure wave that travels through the fluid, which is only visible in the non-protected case because the presence of honeycomb impedes to visualize it. 111 μs after the impact, the projectile is travelling through the fluid while the cavity continues growing. This

is observed in the protected case attending the growing of the non-defined shadow mentioned before. As the cavity increases its size, the fluid pushes the tube walls producing the deformation and the most damaging process in the tube [1, 18, 23]. Approximately 1 ms after the impact the cavity reaches its maximum size, inducing the maximum loading state on the tube walls. That instant can be clearly identified in the images of the non-protected case, whereas in the protected case cannot be seen.

Taking into account the information obtained by the images, it can be concluded that the HRAM process does not change qualitatively by the introduction of the honeycomb protection. However, it is expected that certain phenomena, as cavity expansion, may be affected by it. Due to the fact that the cavity size quantification cannot be made by means of the video images (honeycomb cells impede to have an accurate vision), the HRAM attenuation effect comparison between all the considered cases will be made using the residual deformation and the strain gauge data of the tube walls .

3.2. Tube walls residual deformation

In order to obtain the residual deformation of all the tube walls, it has been used a laser extensometer MEL M27L/50 (Range =50 mm, Resolution=0.2 mm). After the impact, the laser has been attached to an automatic positioning system that is able to sweep the surface of a tube wall. The distance between the laser and each point of the wall is obtained by the laser and registered in a high speed acquisition system (Dewetron DEWE-600) at 1 KHz. Thanks to this distance, it is possible to derive the deformation in all the points of each tube walls, allowing to obtain a contour of the residual deformation. Fig. 5 presents a contour of the

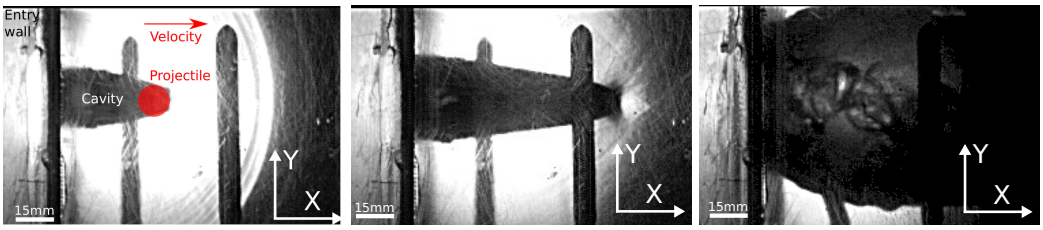

(a) Non-protected $t = 56\ \mu s$ (b) Non-protected $t = 111\ \mu s$ (c) Non-protected $t = 1000\ \mu s$

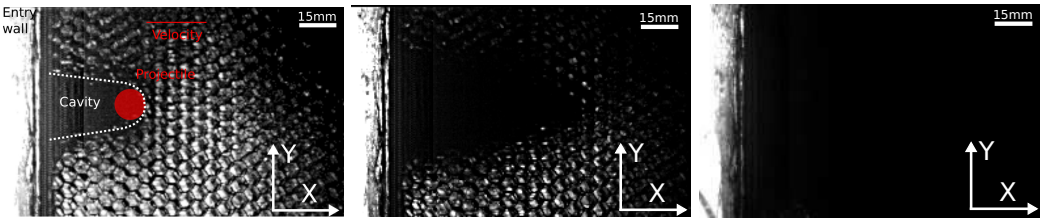

(d) Protected C-1 $t = 56\ \mu s$ (e) Protected C-1 $t = 111\ \mu s$ (f) Protected C-1 $t = 1000\ \mu s$

Figure 4: Video images obtained by the high speed camera

residual deformation of all the tube walls in the non-protected and protected configurations; the crossed-flags in the figure represent a vertical symmetry line. The images clearly show how the deformation is expanded from the impact location in all the cases due to the cavity expansion effect. However it can be seen that both the maximum residual deformation and the area deformed are not the same in the non-protected and protected cases.

The displacements obtained in the non-protected case can be explained taking into account the effects of the cavity evolution on each tube wall. The upper and lower wall (the walls which are not impacted by the projectile) have similar deformation results because they are placed symmetrically with respect to the impact trajectory. The cavity evolves pushing the fluid onto this walls equally. In the entry wall, the deformation is slightly higher than in the upper and lower wall.

The projectile impact produces the failure of the wall and the beginning of the cavity generation, which causes a severe loading around the impact point. It has to be noticed that the final deformation of the entry wall appears in the opposite direction to the projectile velocity. This is explained because the high velocity impact (900 m/s) produces only local deformation around the impact point, while the fluid impulse (which in the entry wall goes in the opposite direction of the projectile) is the governing mechanism that induces the deformation. The exit wall has the highest deformation due to the fact that it is pre-stressed before the impact of the projectile. The projectile, while travels inside the fluid, generates an overpressure ahead which deforms the exit wall before being impacted. Then the impact of the projectile and the cavity expansion continue loading the wall increasing the deformation far from the impact point [16].

Regarding the protected cases, it can be seen that the permanent deformation suffered by the walls follows the same trends as in the non-protected case. This is due to the fact that the phenomena that produce the loading of each wall, previously explained, are the same in these cases. However, it can be noticed a reduction in the permanent deformation for all configurations and tube walls when comparing to the non-protected case. This is produced by the mitigating effect over the cavity expansion that the honeycomb cells produce. The honeycomb cells are deformed by the expansion of the cavity, partially absorbing the energy transferred into the fluid by the projectile and hence reducing the load over the walls. Nevertheless the reduction achieved is not the same for all the protected cases because of the asymmetrical effect created by the orientation of the honeycomb cells in each configuration.

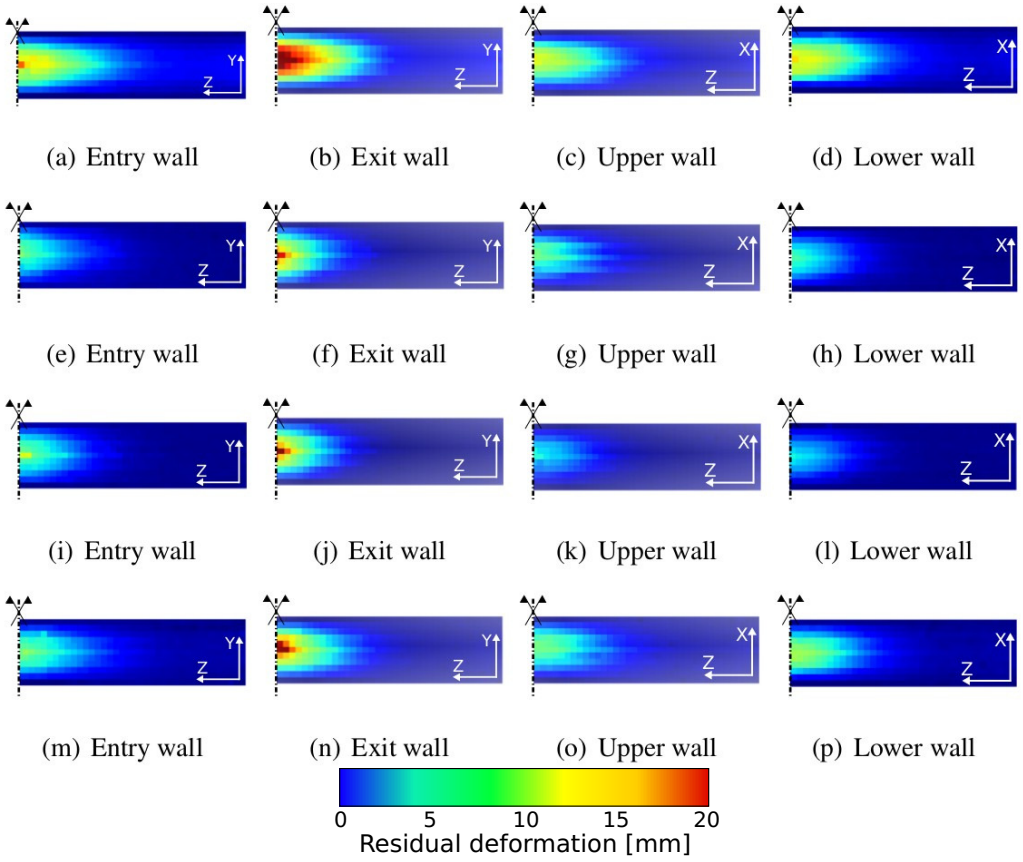

Figure 5: (a)-(d) Non-protected. (e)-(h) Protected C-1. (i)-(l) Protected C-2. (m)-(p) Protected C-3. Contours of permanent out plane deformation plot on aluminium tube walls.

In order to compare quantitatively the different protected configurations studied, Fig. 6 shows the permanent out of plane deformation along the middle path (along axis Z) for all the tube walls (identified in the image with a red line, while impact position is identified with a red arrow). The maximum displacement in all the cases occurs in the central point of the tube, as it was expected. The first thing that can be observed is that, as it was already mentioned, the deformation in all the protected tubes is smaller than in the non-protected case. The differences are

now more evident than in the deformation contours plot showed in Fig. 5. It has to be mentioned that the decrease in the deformation values affects the global shape of the permanent displacement in the walls. Therefore, the honeycomb protection makes the HRAM effect on the walls more located around the impact point. The cavity produced by the projectile in the non-protected case is able to freely expand affecting areas far from the impact point. It can be seen that the non-protected tube shows some permanent deformation on both extreme sides, whereas the protected cases are hardly deformed. This can be important to avoid that the HRAM phenomenon affects contiguous structure elements.

Regarding the honeycomb protected cases, it is observed that in the entry and exit wall (the walls impacted by the projectile) almost no differences appear, although in both cases the honeycomb protected case C-2 slightly shows lower deformations in the walls except in the region close to the holes. The upper and lower wall, however, show a clear difference between the protected cases. The major reduction in the permanent deformation is obtained in the honeycomb case C-2. The configuration C-1 and C-3 show the same results in the upper wall but different in the lower wall because the honeycomb modify slightly the projectile trajectory. As the projectile trajectory may be closer to upper wall than lower, this will increases cavity loading on the wall and therefore deformation. Taken into account the average of the deformation values obtained in the upper and lower walls, it can be concluded that the honeycomb configuration C-3 is the worst in terms of deformation reduction.

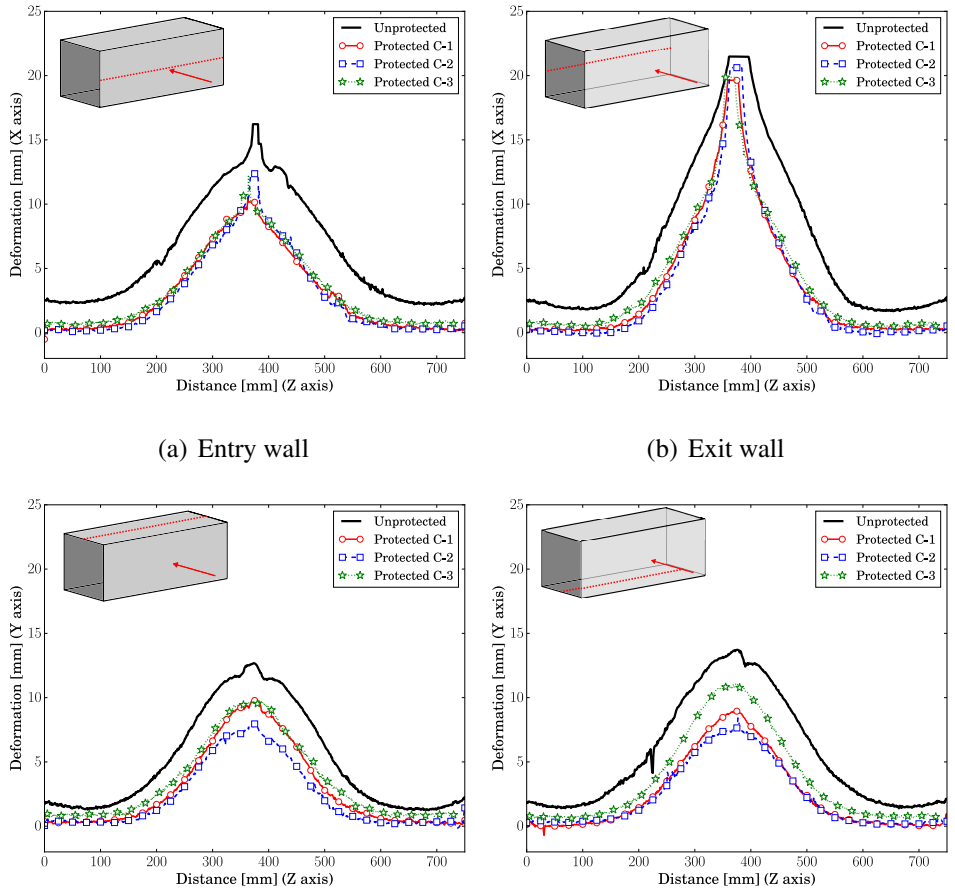

(a) Entry wall

(b) Exit wall

(c) Upper wall

(d) Lower wall

Figure 6: Permanent out of plane deformation in aluminium tube walls

3.3. Strain data in aluminium tube walls

The permanent walls deformation previously studied has shown that the honeycomb protection helps to reduce the HRAM effects. In order to try to understand how the HRAM phenomenon affects the surrounding walls during the impact process, the strain gauges data obtained in the experimental tests have been analysed. Fig. 7 shows the strain time history in different points of the tube walls, for both

non-protected and protected cases. All gauges show that the strain in the non-protected walls is higher than in the protected cases. In the images it is highlighted in red the position of the studied gauge in the tube.

Fig. 7(a) depicts the strain time history of the gauge located near the impact point in the entry wall (gauge G1). It is observed that until approximately 0.18 *ms* the curves are similar for all the configurations, whereas from that instant the strain in the protected configurations is lower than in the non-protected case. This behaviour is due to the fact that in those first instants, the honeycomb does not produced any significant change (neither in the velocity of the projectile nor the phenomena generated) as it was already described attending Fig. 4. Nevertheless, when the cavity starts to grow around the impact point, the honeycomb protection reduce its expansion and hence the loading effect on the entry wall. The strain data shows that the configuration C-2 is the one which exhibits the lowest strain followed by configuration C-3 and finally C-1. The strain time history in this gauge for all the configurations is registered only up to 0.4 *ms* after the impact because the high shake produced by the impact in this zone leads to the debonding of the gauge.

Fig. 7(b) shows the strain time history of the gauge located far from the impact point in the entry wall (gauge G2). Unlike the previous gauge data, all the impact process could be registered because in this region (150 *mm* far from the impact point) the shake is lower, avoiding the debonding of the gauge. As happened before, it can be distinguished a first region in which the differences between the configurations are not clear (until 0.7 *ms* approximately) and a second region

where is clearly observed the reduction in the strain for the protected cases. These two regions are related, as was already explained, to the cavity evolution and its influence on the loading walls effect at different distances from the impact point. In this case, as the gauge G2 is far from the impact point, the effect of the cavity in the strain takes a longer time than in the case of G1. In addition, as the cavity finds more honeycomb cells on its path, the honeycomb protection produces a higher reduction on the strain values than in the case of the gauge G1. It can be observed how the maximum strain value is obtained in the non-protected case at 1.5 ms after the impact; close to the instant where the cavity reaches its maximum size ($\sim$ 1 ms). Therefore, the maximum loading effect on the surrounding structure can be related to the the maximum cavity expansion. Due to the attenuation effect of the honeycomb structure, the strain registered in the protected cases is lower and the maximum is reached sooner. Once the cavity has reached its maximum size it starts to diminish, and the strain value is reduced due to the elastic recovery of the wall. Finally, the data reaches a plateau that corresponds to the plastic deformation of the tube. The protected configuration with the lowest strain values is again C-2.

Regarding the strain in the exit wall, Fig. 7(c) shows the data obtained by the gauge located far from the impact point (at the same position as gauge G2). It is observed that the strain data is similar to the one registered in G2, previously analysed. It can be seen also that up to $\sim$ 1 ms all the cases show similar results. This duration is controlled mainly by the impact to the exit wall and the initiation of the cavity expansion. This observation could lead to think that projectile velocity is not altered significantly by the presence of the honeycomb structure.

However, when maximum cavity expansion takes place, the results show again that the protected configurations mitigate the HRAM effects on the tube. The strain time history obtained in the gauge located near the impact point in the exit wall (gauge G3) does not provide useful information because in all the cases the gauge is debonded few microseconds after the projectile hits the mentioned wall.

Finally,Fig. 7(d) shows the strain time history of the gauge located in the central point of the upper wall (which is not impacted by the projectile). It is observed that the strain values are higher in this point than in the other gauges. This is probably due to the fact that the gauge is located just above the projectile path and in a place where the cavity reaches its maximum size, producing a severe loading on the upper wall. At approximately 0.5 ms after the impact the gauge for the non-protected case and for the configuration C-1 are debonded due to the high impulse generated by the cavity. This does not happen in the other configurations, which would corroborate the HRAM mitigating effect of those protected cases. It can be seen that the protected configuration C-2 obtains the major reduction of strain once the cavity is totally expanded ($\sim$ 1 ms), before than in the non-protected case as was previously explained and showing a lower residual strain, confirming all the previous finding obtained for the permanent deformation.

The results shown in Fig. 6 and 7 indicate that the honeycomb protection is able to reduce the deformation of the walls, and therefore the vulnerability of the tubes subjected to the HRAM phenomenon. It has been observed that the best protected configuration in terms of deformation and strain reduction is the configuration C-2. In order to analyse the attenuation of the HRAM effects achieved by this configuration, it is obtained a contour map which represents the reduction

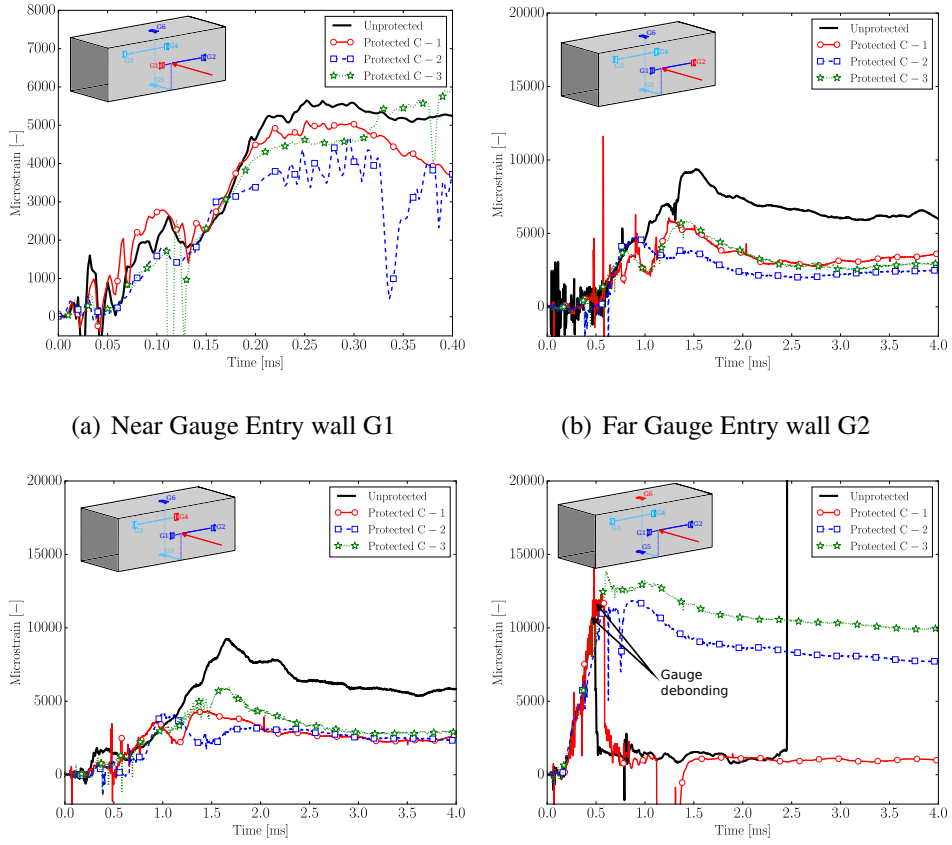

(a) Near Gauge Entry wall G1

(b) Far Gauge Entry wall G2

(c) Far Gauge Exit wall G4

(d) Gauge Upper wall G6

Figure 7: Strain gauge information

of permanent deformation in the different tube walls of the protected case C-2, compared to the non-protected case (Fig. 8). It can be observed that the major reductions are obtained near the impact point of the exit wall, which is where the maximum deformation of the tube appears. Nevertheless, taking into account the reduction of maximum deformation in each wall, it can be concluded that the higher attenuation is reached in the lower wall, where a reduction of 46% (compared to the non-protected case) is obtained. Therefore it can be concluded that

the attenuation effect is more important, in relative terms, where the cavity expansion is the main loading case. It has to be mentioned that the pictures show some asymmetrical differences in the results, because as it was explained earlier the honeycomb could induce slight differences on projectile trajectory.

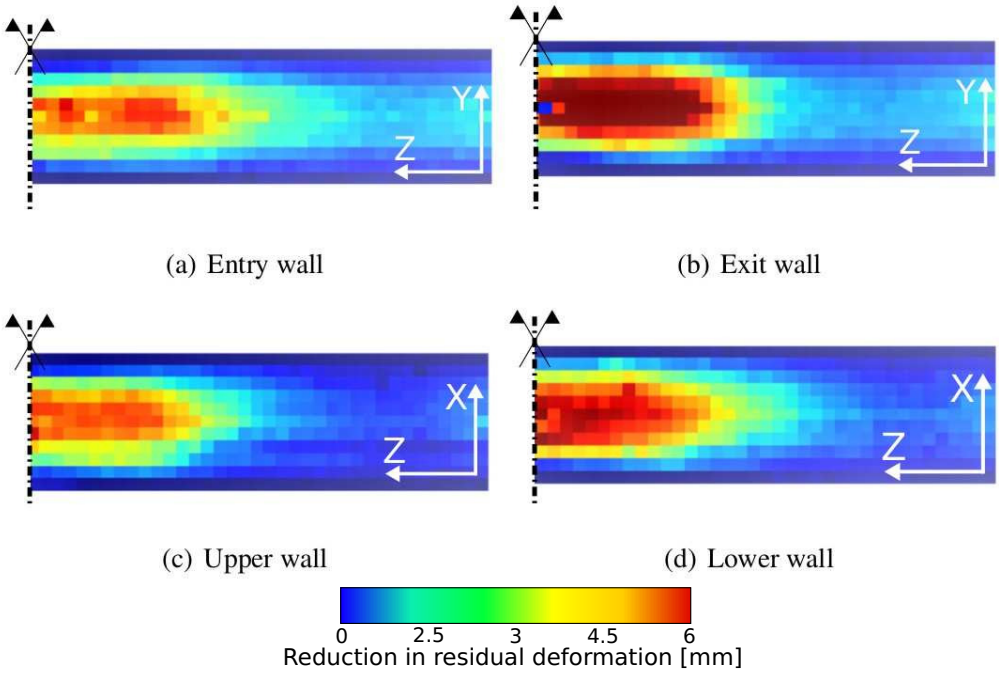

(a) Entry wall (b) Exit wall

(c) Upper wall (d) Lower wall

Figure 8: Reduction in the deformation tube walls.

4. Analysis of the HRAM attenuation method

In light of the results previously shown, it can be concluded that the honeycomb panels reduce the vulnerability of a structure subjected to the HRAM phenomenon. First of all, it is necessary to clarify if the attenuation produced by the honeycomb is due to the projectile deceleration generated by the resistance of the honeycomb to its penetration (lower projectile velocity means lower cavity

406 expansion) or to the resistance of the honeycomb to the expansion of the cavity.
407 To this end a simple analytical model has been implemented to model the de-
408 celeration of the projectile on a protected and non-protected configuration. The
409 deceleration produced by the fluid has been obtained according to the drag of a
410 spherical projectile inside a fluid (more information can be found in [1] where the
411 present approach is validated). The deceleration obtained on the aluminium tube
412 walls and in the honeycomb thin walls has been obtained using the energy balance
413 equation for piercing penetration [34, 35]. The number of honeycomb thin walls
414 has been obtained to model each impact on each honeycomb thin wall. For the
415 model, only the worst case in which the projectile perforates all the cell walls has
416 been taken into account.

417 In Fig. 9 it can be seen the projectile velocity with respect the projectile dis-
418 placement for a non-protected and a protected configuration. It can be seen that
419 velocity differs gradually with the displacement up to a maximum reduction on
420 the final velocity of only $\sim 30\, m/s$ in the protected configuration. Moreover in
421 the first instant of the impact, where the velocity is higher and the cavity starts
422 to evolve, velocity differences are negligible. These observations confirm that the
423 projectile velocity is hardly affected by the presence of the honeycomb. Therefore
424 the major role on the HRAM attenuation effects is due to the honeycomb resis-
425 tance to cavity expansion.

426

427 In order to analyse how the honeycomb attenuates the HRAM effects and to
428 understand the differences between the protected configurations tested, regarding
429 the mitigation effect obtained, it is studied the honeycomb structure deformation
430 inside the tube. Finally, an analysis relating the cavity size and the tube wall de-

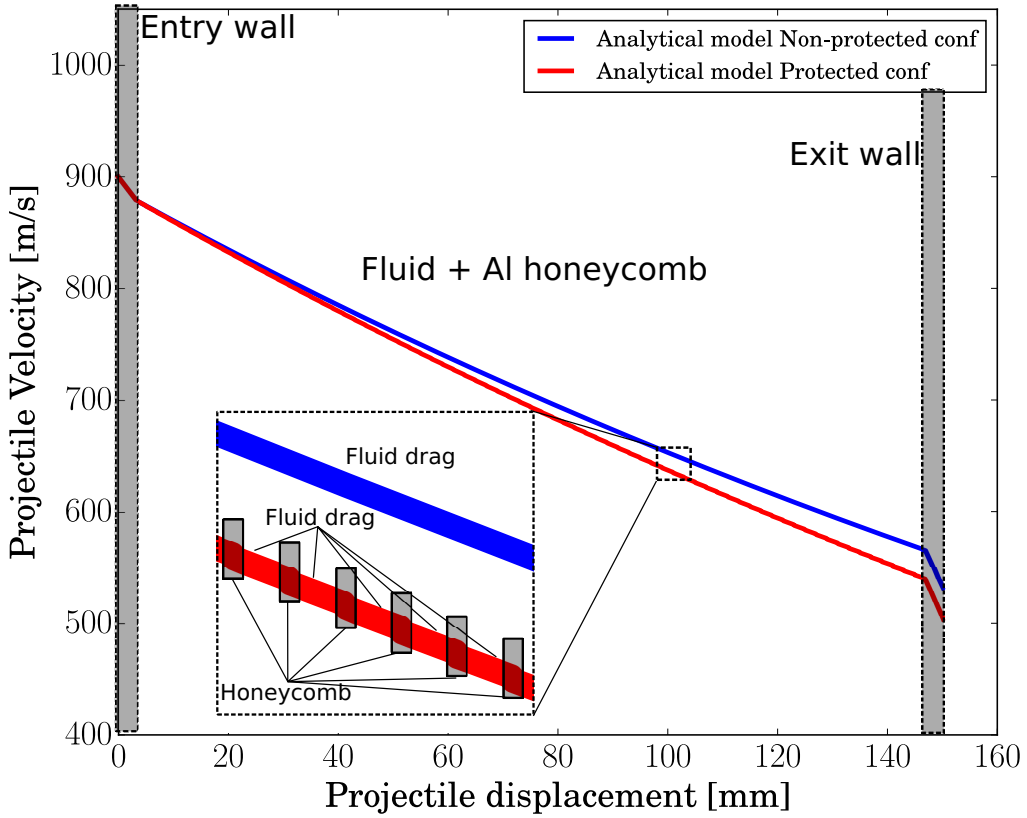

Figure 9: Analytical model for velocity deceleration.

formation is performed.

4.1. Honeycomb structure deformation

In order to analyse the honeycomb structure deformation produced by the HRAM loading, the tubes and the honeycomb structure are cut in two halves in a plane that is perpendicular to the longitudinal direction of the tube (Z axis) and that contains the projectile path. The cut has been done using a circular saw taking care of not modifying the damage and deformation produced during the impact.

The analysis has been conducted in order to understand the performance of each configuration.

Fig. 10 shows a normal view and a perspective view of the cut plane for all the protected configurations tested. It is included also the maximum dimension of the deformed honeycomb structure in the different axes. The images of the configuration C-1 show very clearly how the honeycomb has been deformed along the projectile path. The projectile impacts the tube and perforates all the honeycomb cells in its path. As it is seen in Fig. 9 neither projectile velocity nor the trajectory is affected noticeable by the presence of the honeycomb. As the projectile travels through the tube, the cavity generated on its trajectory evolves and deforms the impacted honeycomb panel that try to avoid its expansion. Due to this loading the impacted honeycomb panel is broken in two parts and its deformation occurs mainly in the lower-upper tube walls direction (Y axis). The fluid is able to flow through the cells oriented in the longitudinal direction of the tube (Z axis), so the damage of those adjacent honeycomb panels is much lower (only honeycomb cell debonding can be observed). It has to be noted that in this configuration 15 honeycomb panels of 50 *mm* are used to fill the entire space of the tube, being the cells oriented in the longitudinal direction of the tube (Z axis). Therefore due to the absence of connection between the different panels, the deformation produced by the cavity expansion does not reach the adjacent ones. It has to be remarked that the use of other thickness for the panel will probably have influence on the results.

Regarding the honeycomb structure deformation, it can be said that the main absorbing energy mechanism is the bending of thin honeycomb walls [36, 37, 38],

but also some energy is dissipated by the debonding of the honeycomb cells in the adjacent panels. Certainly this energy transferred from the fluid to the honeycomb structure alleviates the tube loading, mitigating the HRAM effects. Finally, the similarity between the shapes of the honeycomb deformation and the cavity, leads to think that the maximum expansion of the cavity is similar to the maximum deformation of the honeycomb panel. This could be a design key to know which solution or configuration could contribute in a better way to improve the vulnerability of a structure, because the smaller the cavity, the lower would be the deformation of the structure.

It has been previously seen that the protected configuration C-2 shows the best results in terms of reduction of residual displacement. This configuration consists of three honeycomb panels with the cells oriented parallel to the projectile trajectory (X axis). Fig. 10 shows that the three honeycomb panels are equally deformed along the projectile path. The projectile impacts the tube and travels through the honeycomb cells while the cavity try to evolve radially deforming the honeycomb cells that are all around it. The cavity is much more restricted in this configuration than in configuration C-1 or C-3, because in the other cases the honeycomb cell direction matches with one radial direction of the cavity expansion. The images show that for this configuration the dominant failure mechanism is cell wall buckling, which leads to a higher resistance. Thus the energy dissipated by the honeycomb occurs in a more efficient way for configuration C-2. This would explain why the better results are obtained with this configuration. Although in this case the cells allow the fluid to flow in the projectile direction, the results obtained in the entry and exit walls are similar to the other protected cases. This

could be explained due to the fact that the deformation in these walls is mainly influenced by the projectile impact and the fluid impulse around the impact point, effects that are negligibly affected by the different configurations of the honeycomb.

Finally, the honeycomb panels deformation for the protected configuration C-3 can also be observed in Fig. 10. This configuration consists of three honeycomb panels with the cells oriented in the lower-upper wall direction of the tube (Y axis). It is observed that the honeycomb deformation appears mainly in the middle panel, which matches with the projectile path. The cavity evolves pushing the honeycomb wall cells towards the longest tube direction (Z axis). The images show that as it occurs in configuration C-1, bending of thin honeycomb wall is the dominant failure mechanism. Due to the orientation of the cells, the fluid can flow in the lower-upper wall direction without generating a significant deformation on the adjacent honeycomb panels, like in the configuration C-1. This could explain the smaller reduction of deformation in the upper and lower walls for the protected configuration C-3. Taking into account the orientation of the cells, it could be thought that the entry and exit walls would be more protected because the cavity expansion is restricted in those directions, nevertheless the residual displacement and gauges show very few differences. As it was already explained, the effect of the honeycomb is less noticeable in these walls since the projectile velocity is hardly affected.

The analysis of the honeycomb deformation performed shows that the protected configuration C-2 achieves the better attenuation results, especially in the

upper and lower walls, because the cavity expansion is more restricted due to in this configuration cell wall buckling is the dominant failure mechanism, increasing honeycomb resistance. It can be concluded that the energy dissipated by the deformation of the honeycomb produces a reduction in the energy transferred to the structure, attenuating the HRAM effects and reducing the vulnerability of a structure subjected to the HRAM phenomenon.

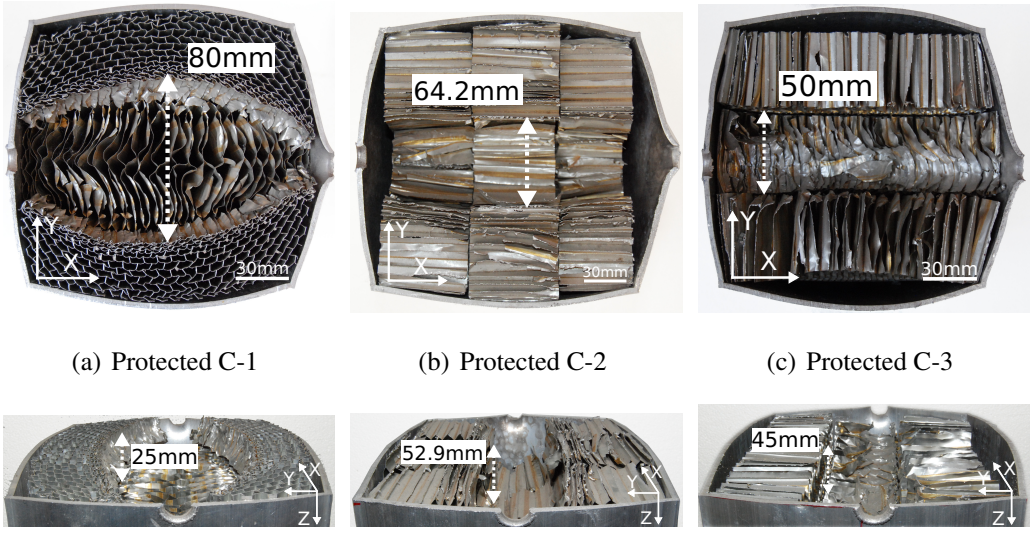

(a) Protected C-1 (b) Protected C-2 (c) Protected C-3

(d) Protected C-1 (e) Protected C-2 (f) Protected C-3

Figure 10: Images of the cut plane of each protected configuration

4.2. Cavity size and tube walls deformation

Finally, it is performed an analysis relating the cavity size and the tube walls deformation. In the Fig. 12 the volume of the estimated cavity is compared with the volume generated by the expansion of the tube walls.

Concerning the volume of the cavity, as it was already commented, the maximum cavity size can be obtained for the non-protected case by means of the high speed camera. As it can be seen in Fig. 11, the cavity geometry is similar to an ellipsoid and therefore its axes can be obtained from this image. In the upper-lower wall direction (Y axis) the size of the cavity is 120 *mm*, while in the entry-exit wall direction (X axis) the size is obtained as the final deformed distance between these walls in the projectile trajectory (190 *mm*). The images does not show the size in the longitudinal tube direction (Z axis), but according to other works [17, 23, 16] in which similar cases have been studied numerically, it can be established that this size is the same as in the upper-lower wall direction (Y axis). In the protected cases, as it has been said previously, the honeycomb panels avoid viewing the inside of the tube. However taking into account the similarity between the shapes of the honeycomb deformation and the expected cavity, it has been made the hypothesis that the maximum expansion of the cavity matches with the maximum deformation of the honeycomb panel (already detailed in Fig. 10). It has to be mentioned that this hypothesis cannot be made in the honeycomb cell direction since the fluid can flow freely across them and only slight honeycomb cell debonding is observed. In this direction it is expected that the size of the cavity does not show any noticeable alteration with the non-protected case.

Concerning the volume of the tube walls generated by the expansion of the cavity, the value has been obtained using the expanded displacement shown in Fig. 5. In order to obtain the contour, each wall is divided in 11×75 regions. Therefore, each region represents an area of $13.63 \times 10\ mm \times mm$, where the averaged value of the out of plane residual deformation is obtained. The volume

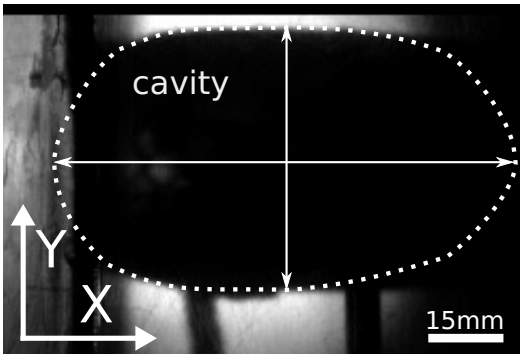

Figure 11: Video images obtained by the high speed camera. Non-protected $t = 472\ \mu s$

generated has been obtained adding all the region averaged value of the residual deformation and multiplying by the region surface.

As it can be seen in Fig. 12, there is an adequate correlation between both volumes. This trend confirms the main hypothesis of the work in which the reduction of cavity expansion by the use of the honeycomb alleviates the loading level of the structure. Moreover, it confirms that the hypothesis made to obtain the volume of the cavity in the protected cases are well established. It can be seen that an important reduction of the wall displacement volume is obtained due to the reduction of the cavity size for all protected configurations. As it can be seen previously, the best performance is exhibited for the configuration C-2, followed by C-1 and finally C-3. C-2 configuration is able to obtain a reduction of a 54% in terms of the expanded volume of the walls produced by a similar reduction of the cavity size.

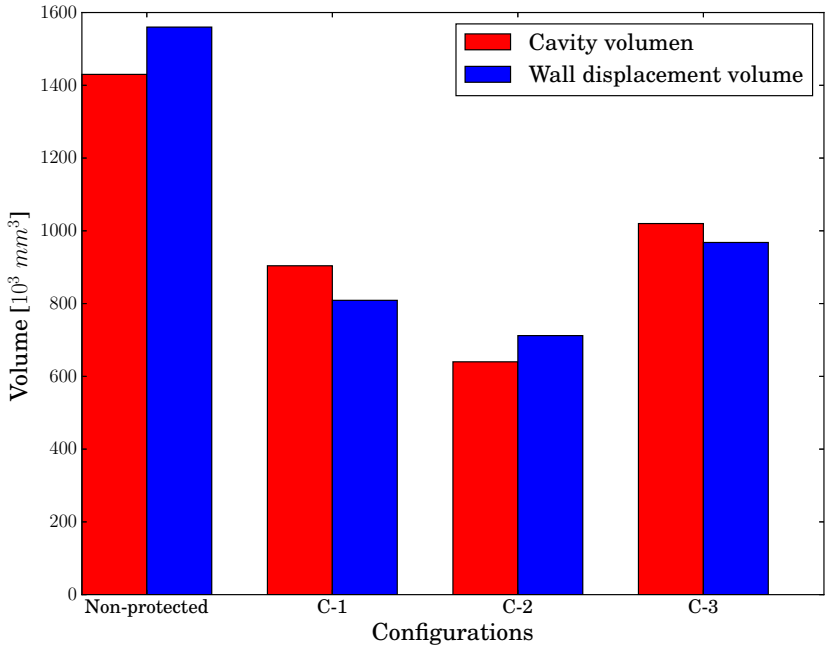

Figure 12: Reduction in the deformation tube walls and in the cavity expansion

5. Conclusion

In this work a method of HRAM attenuation is proposed. The solution tackles the expansion of the cavity, which has been shown in previous studies as the most damaging event of the HRAM phenomenon when the size of the cavity is similar to the size of the tube. The method consists in placing honeycomb panels inside the fluid filled structure that is subjected to the HRAM phenomenon . Three different configurations have been studied comparing the results to the non-protected configuration, leading to the following conclusions.

- The proposed method does not alter qualitatively the different phases of the HRAM. It has been shown that the cavity expansion is restricted by this device and therefore it is obtained smaller residual deformation in the tube,

and consequently a less damaging phenomenon.

- The proposed attenuation method does not counteract the effort in reducing the weight on aircraft structures due to low honeycomb density. Moreover, the honeycomb cell size assures a correct filling and circulation of water inside them.

- All the protected configurations achieve a negligible deformation far enough from the impacted point, reducing the possible damage that can be produced on adjacent structures.

- It has been shown that the reduction of cavity expansion matches almost perfectly with the reduction of residual deformation. This fact confirms that for this geometry the cavity is the most damaging phase in the HRAM phenomenon. It has to be remarked that for other structure geometries, in which the tube is much bigger and the cavity expansion is not the most damaging event, other methods have to be studied and compare it with the present one to analyse which is the most efficient one.

- Once studied the three configurations, it has been seen that the most efficient one is the protected configuration C-2. This is explained because it is the one that is able to restrict the cavity expansion in a more efficient way, limiting it in the two perpendicular direction of projectile trajectory.

- The orientation of the panel has been proven as the key parameters to optimize attenuation purposes for these impact conditions. However, as it can be seen for configuration C-1 other variables as the thickness of the panel may have an additional effect on the protection performance.

- For the best configuration, it has been obtained up to a 54 % of reduction in the expanded wall displacement volume produced by a similar reduction in the cavity size. Therefore the attenuating effect of the HRAM phenomenon is successfully reached.

Acknowledgements

This research was done with the financial support of the Vicerrectorado de Política Científica UC3M (Projects 2014/00006/002 and 2013/00413/002).

References

[1] D. Varas, J. López-Puente, R. Zaera, Experimental analysis of fluid-filled aluminium tubes subjected to high-velocity impact, Int. J. Impact Eng. 36 (1) (2009) 81 – 91.

[2] J. G. Avery, Design manual for impact damage tolerant aircraft structure, Technical report AGARD-AG-238 (1981).

[3] M. J. Jacobson, Addendum to design manual for impact damage tolerant aircraft structure, Technical report AGARD-AG-238 (Addendum) (1988).

[4] V. Authors, In-flight uncontained engine failure airbus a380-842, VH-OQA, Technical report Australian Transport Safety Bureau (2010).

[5] N. Moussa, M. Whale, D. Groszmann, , X. Zhang, The potential for fuel tank fire and hydrodynamic ram from uncontained aircraft engine debris, Report DOT/FAA/AR-96/95 Federal Aviation Administration (1997).

[6] J. Pernas-Sánchez, J. Artero-Guerrero, D. Varas, J. López-Puente, Experimental analysis of ice sphere impacts on unidirectional carbon/epoxy laminates, Int. J. Impact Eng. 96 (2016) 1 – 10.

[7] M. Anghileri, L.-M. L. Castelletti, F. Invernizzi, M. Mascheroni, A survey of numerical models for hail impact analysis using explicit finite element codes, Int. J. Impact Eng. 31 (8) (2005) 929 – 944.

[8] A. Airoldi, B. Cacchione, Modelling of impact forces and pressures in lagrangian bird strike analyses, Int. J. Impact Eng. 32 (10) (2006) 1651 – 1677.

[9] R. Mines, S. McKown, R. Birch, Impact of aircraft rubber tyre fragments on aluminium alloy plates: I-experimental, Int. J. Impact Eng. 34 (4) (2007) 627 – 646.

[10] V. Authors, Accident on 25 july 2000 at la patte d'oie in gonesse to the concorde registered f-btsc by air france, Ministere de l' équipement des transports et du logement Buereau d'enquetes et d'analyses pour la secourite de l'aviation civile (2000).

[11] N. Lecysyn, A. Dandrieux, F. Heymes, P. Slangen, L. Munier, E. Lapebie, C. L. Gallic, G. Dusserre, Preliminary study of ballistic impact on an industrial tank: Projectile velocity decay, J. of Loss Prevent. Proc. 21 (6) (2008) 627 – 634.

[12] N. Lecysyn, A. Dandrieux, F. Heymes, L. Aprin, P. Slangen, L. Munier, C. L. Gallic, G. Dusserre, Ballistic impact on an industrial tank: Study and modeling of consequences, J. Hazard. Mater. 172 (2-3) (2009) 587 – 594.

[13] N. Lecysyn, A. Bony-Dandrieux, L. Aprin, F. Heymes, P. Slangen, G. Dusserre, L. Munier, C. L. Gallic, Experimental study of hydraulic ram effects on a liquid storage tank: Analysis of overpressure and cavitation induced by a high-speed projectile, J. Hazard. Mater. 178 (1-3) (2010) 635 – 643.

[14] P. J. Disimile, L. A. Swanson, N. Toy, The hydrodynamic ram pressure generated by spherical projectiles, Int. J. Impact Eng. 36 (6) (2009) 821 – 829.

[15] E. Deletombe, J. Fabis, J. Dupas, J. Mortier, Experimental analysis of 7.62 hydrodynamic ram in containers, J. Fluid. Struct. 37 (2013) 1 – 21.

[16] D. Varas, R. Zaera, J. López-Puente, Numerical modelling of the hydrodynamic ram phenomenon, Int. J. Impact Eng. 36 (2006) 363–74.

[17] J. Artero-Guerrero, J. Pernas-Sánchez, D. Varas, J. López-Puente, Numerical analysis of CFRP fluid-filled tubes subjected to high-velocity impact, Compos. Struct. 96 (2013) 286 – 297.

[18] T. Fourest, J.-M. Laurens, E. Deletombe, M. Arrigoni, J. Dupas, Cross validation of analytical and finite element models for hydrodynamic ram loads prediction in thin walled liquid filled containers, J. Fluid. Struct. 59 (2015) 285 – 296.

[19] S. Heimbs, A. Nogueira, E. Hombergsmeier, M. May, J. Wolfrum, Failure behaviour of composite t-joints with novel metallic arrow-pin reinforcement, Compos. Struct. 110 (2014) 16 – 28.

[20] T. Fourest, J.-M. Laurens, E. Deletombe, J. Dupas, M. Arrigoni, Analysis

of bubbles dynamics created by hydrodynamic ram in confined geometries using the rayleigh-plesset equation, Int. J. Impact Eng. 73 (2014) 66 – 74.

[21] D. Varas, R. Zaera, J. López-Puente, Numerical modelling of partially filled aircraft fuel tanks submitted to hydrodynamic ram, Aerosp. Sci. Technol. 16 (1) (2012) 19 – 28.

[22] D. Varas, J. López-Puente, R. Zaera, Numerical analysis of the hydrodynamic ram phenomenon in aircraft fuel tanks, AIAA J. 50 (7) (2012) 1621–1630.

[23] J. Artero-Guerrero, J. Pernas-Sánchez, J. López-Puente, D. Varas, On the influence of filling level in CFRP aircraft fuel tank subjected to high velocity impacts, Compos. Struct. 107 (2014) 570 – 577.

[24] A. Copland, Hydrodynamic ram attenuation, US Army Ballistic Research Laboratory. ARBRL-MR-03246 (1983).

[25] S. McCormick, P. F. Motzenbecker, M. J. Clauson, Study of passive fuel tank inerting systems for ground combat vehicles, U.S. ARMY TANK-AUTOMOTIVE COMMAND RESEARCH, DEVELOPMENT AnD ENGINEERING CENTER. AD-A201 403 (1988).

[26] D. Townsend, N. Park, P. M. Devall, Failure of fluid dilled structures due to high velocity fragment impact, Int. J. Impact Eng. 29 (1-10) (2003) 723 – 733.

[27] P. J. Disimile, J. Davis, N. Toy, Mitigation of shock waves within a liquid filled tank, Int. J. Impact Eng. 38 (2011) 61–72.

[28] G. Sun, H. Jiang, J. Fang, G. Li, Q. Li, Crashworthiness of vertex based hierarchical honeycombs in out-of-plane impact, Mater. Design 110 (Supplement C) (2016) 705 – 719.

[29] D. Wang, Impact behavior and energy absorption of paper honeycomb sandwich panels, Int. J. Impact Eng. 36 (1) (2009) 110 – 114.

[30] S. R. Bates, I. R. Farrow, R. S. Trask, 3d printed polyurethane honeycombs for repeated tailored energy absorption, Mater. Design 112 (Supplement C) (2016) 172 – 183.

[31] L. Hu, X. He, G. Wu, T. Yu, Dynamic crushing of the circular-celled honeycombs under out-of-plane impact, Int. J. Impact Eng. 75 (Supplement C) (2015) 150 – 161.

[32] F. Sun, C. Lai, H. Fan, In-plane compression behavior and energy absorption of hierarchical triangular lattice structures, Mater. Design 100 (Supplement C) (2016) 280 – 290.

[33] M. Nishida, K. Tanaka, Experimental study of perforation and cracking on water filled aluminum tube impacted by steel spheres, Int. J. Impact Eng. 32 (2006) 2000–2016.

[34] P. Hazell, Armour: Materials, Theory, and Design, CRC Press, 2015.

[35] D. Carlucci, S. Jacobson, Ballistics: Theory and Design of Guns and Ammunition, Third Edition, CRC Press, 2018.

[36] M. Vural, G. Ravichandran, Microstructural aspects and modeling of failure

in naturally occurring porous composites, Mechanics of Materials 35 (3) (2003) 523 – 536.

[37] B. Koohbor, S. Ravindran, A. Kidane, Effects of cell-wall instability and local failure on the response of closed-cell polymeric foams subjected to dynamic loading, Mechanics of Materials 116 (2018) 67 – 76, iUTAM Symposium on Dynamic Instabilities in Solids.

[38] L. Gibson, M. Ashby, Cellular Solids: Structure and Properties, Cambridge Solid State Science Series, Cambridge University Press, 1999.